# Noninvasive Measurement of Membrane Potential Modulation in Microorganisms: Photosynthesis in Green Algae

**Eun-Hee Lee, Seung-Woo Lee, and Ravi F. Saraf***

Chemical and Biomolecular Engineering, University of Nebraska-Lincoln, Lincoln, Nebraska 68588, United States

**ABSTRACT** Cell membrane potential (CMP) modulation is a physical measurement to quantitatively probe cell physiology in real time at high specificity. Electrochemical field effect transistors (eFETs) made from graphene and Si nanowire provide strong mechanical and electrical coupling with neurons and muscle cells to noninvasively measure CMP at high sensitivity. To date, there are no noninvasive methods to study electrophysiology of microorganisms because of stiff cell walls and significantly smaller membrane polarizations. An eFET made from the smallest possible nanostructure, a nanoparticle, with sensitivity to a single-electron charge is developed to noninvasively measure CMP modulation in algae. The applicability of the device is demonstrated by measuring CMP modulation due to a light-induced proton gradient inside the chloroplast during photosynthesis. The ~9 mV modulation in CMP in algae is consistent with the absorbance spectrum of chlorophyll, photosynthetic pathway, and inorganic carbon source concentration in the environment. The method can potentially become a routine method to noninvasively study electrophysiology of cells, such as microorganisms for biofuels.

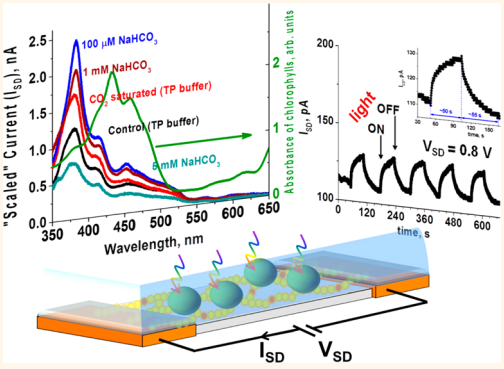


**KEYWORDS:** cell membrane potential · photosynthesis · single electron transistor · electrochemical transistor · nanoparticle array

Most biochemical processes, such as cell growth, nutrient uptake, energy production, and cell signaling, involve the transport of ions through membranes. Monitoring the cell membrane potential (CMP) is a powerful physical measurement to quantitatively study cell physiology at high specificity, such as cell signaling, respiration and photosynthesis, metabolism, action potential propagation, and muscle contraction. The membrane potential, which reflects the sum of all electric transport processes, is measured by inserting delicate micropipet electrodes[1−3] and ultramicroelectrodes[4] that often damage the cell. These methods of directly measuring the membrane voltage, or current, are tedious and invasive with less than a 5% success rate due to cell damage. A noninvasive method of using voltage-sensitive dyes,[5,6] is indirect with low sensitivity.

Micron-scale field-effect transistors (FETs) have been studied and developed over the past two decades,[7−9] and they are able to directly measure cell membrane potential (CMP) noninvasively by simply depositing (i.e., seeding) neurons[10] and cardiac muscle[11] cells on the device (gate) electrode. Although the mammalian cells are soft and conform to the device surface, the formation of a cleft at the interface is a key challenge that complicates the analysis and adversely affects the quality of the signal and responsiveness of the FET.[12−14] A strong coupling with a low cleft leads to lower contact impedance and, therefore, lower noise and a higher signal.[14] Modification of the planar electrode with nanostructures, such as Au nanopillars[15] and carbon nanotubes (CNTs),[16] improves the signal, and the contact impedance decreases 15- to 20-fold for CNT-modified electrodes.[17] The decrease is even greater for nanostructured metal electrodes.[18,19]

Taking advantage of better coupling, the FET principle was extended, less than a decade ago, to make nanoscale eFETs using

* Address correspondence to rsaraf2@unl.edu.

Received for review October 17, 2013 and accepted December 19, 2013.

**Published online December 19, 2013**
**10.1021/nn405437z**

graphene[20,21] and Si nanowires[20,22] to record ion channel activity in neurons and heart muscle cells. (We note in passing that an eFET is a FET where the current is gated by an electrolyte, *i.e.*, the modulation in the ion concentration in the electrical double layer (EDL) changes the conductance of the device.)[23] The performance is enhanced for nano-eFETs over micro-FETs owing to tighter cell/device coupling[24,25] and higher sensitivity to interfacial charge modulation on cell membrane depolarization.[26] The soft mammalian cell is deposited on graphene or nanowire interposed between two electrodes (source and drain) at a distance $L$ apart. At a constant bias between the source and drain, $V_{SD}$, on cell stimulation, the device current ($I_{SD}$) through the nanostructure modulates because of the changes in the CMP (*i.e.*, gating). The CMP modulation, $\Delta\varphi = \Delta I_{SD}/g_m$, where, $\Delta I_{SD}$ is the change in device current and $g_m$ is an easy-to-measure property of eFETs called transconductance. Transconductance is the sensitivity of the eFET. The sensitivity, $g_m$ is $\sim 1/L^2$ and $\sim 1/L$ for nanowire[26] and graphene[27] FET devices, respectively. As a result, the sensitivity ($g_m$) drops rapidly in the $\leq 10^0$ nS range as $L$ is increased above 50 $\mu$m,[28,29] a practical size to conveniently deposit (seed) mammalian cells or microorganisms for routine analysis. Furthermore, noninvasive CMP measurements on microorganisms remain a challenge because their rigid cell walls make it difficult for conformal contact, and $\Delta\varphi$ is in mV range compared to tens of mV for neurons and muscle cells (studied for graphene and nanowire devices).

We report, for the first time, robust coupling of an eFET to measure the CMP of a microorganism. The CMP of green algae (*Chlamydomonas reinhardtii*) is measured during photosynthesis of $\Delta\varphi$ in the $10^0$ mV range. The response to light is consistent with the absorbance spectrum of chlorophyll, photosynthesis pathway, and optimum carbon concentration in the environment. The eFET is made from a two-dimensional (2D) network array of one-dimensional (1D) nanoparticle necklaces with $L \approx 70$ $\mu$m. The 1D necklace topology of 10 nm particles leads to single electron sensitivity and, at the same time, provides connectivity to the electrodes and cell at $L > 50$ $\mu$m.[30−32] In a previous study, the necklace array, as a FET sensor operating in air, was shown to successfully record the metabolic activity in yeast cell stimulated by methanol vapor.[30] The signal was generated from the redox of the exocytosis of formaldehyde on the array. Recently, for the first time, a single-electron eFET operating in water was demonstrated by nanocementing the adjacent particles in the necklace with iron oxide.[32] Using the nanocemented necklace array, here, the application to measure the CMP of a microorganism during photosynthesis is reported. The single-electron eFET depends on the number of (single-electron) charge centers in the percolation path of the necklace array;[33] thus, in contrast to nanowire and graphene eFETs, increasing $L$ will enhance the sensitivity of the nanoparticle array device.[34] Unlike the previous study on chemical stimulation of yeast in air,[30] the gating is by physical stimuli (i.e., light) with no exocytosis of redox moieties. The light stimulation in photosynthesis avoids the complexities associated with mass transfer limitations during chemical stimulation processes.

## RESULTS AND DISCUSSION

The single-electron eFET, schematically shown in Figure 1a, is fabricated as follows. The nanoparticles spontaneously form a 1D necklace in solution by slowly adding a salt solution (see Methods). The "polymerization" of the nanoparticles to form a 1D necklace results in a remarkable change in the color of the solution due to red-shift in the surface plasmon resonance peak, as described previously for other systems[30,35] (see Supporting Information (SI) Figure A). The necklace array is patterned between two Au electrodes, 50 and 70 $\mu$m apart on a $SiO_2$(500 nm)/Si chip, by soft lithography.[32,35] The necklace "climbs" over the electrode to form a good contact (Figure B, SI). For the single-electron eFET, the electrodes are hermetically sealed with an adhesive (Figure 1a).[32] The unicellular algae are cultured in a tris-acetate-phosphate medium (TAP, pH 7.2) and deposited on the necklace array by simple dip coating (Figure 1b). The monolayer of algae between the electrodes forms a good interface with the underlying nanoparticle necklace array (Figure 1e). There are approximately 20 cells on the necklace array in the electrode gap. Without the necklace array, there is no interconnection between the two hermetically sealed electrodes in the solution. The procedures for creating the necklace synthesis, algae culture, and the eFET device are briefly described in the Methods section. The biogating experiment is to apply a constant bias, $V_{SD}$, between the electrodes and measure the current, $I_{SD}$, through the necklace array (Figure 1a). Algal cell deposition and measurement only took ~20 min on each sample.

Without the cells, at constant bias, $V_{SD}$, the $I_{SD}$ does not change with exposure to light. On modulating the potential between the solution and the array, $V_g$, the device current at fixed $V_{SD}$ changes (Figure 2a). From the derivative of the $V_{SD}$ *versus* $I_{SD}$ characteristics, the transconductance, $g_m = |dI_{SD}/dV_g|$, of the device (without the cells) at $V_{SD} = 0.8$ V is obtained. The transconductance is the sensitivity of the device that prescribes the change in current due to modulation in the environment potential (*i.e.*, $V_g$). Importantly, at $V_g = 0$, $g_m \approx 2.3$ is significant to operate the eFET with no external gating power supply at $V_g = 0$. This is in contrast to graphene- and nanowire-based devices,[28,29] where $V \neq 0$ makes the estimation of $\Delta\varphi$ more complicated.

On deposition of the cells, the device becomes light sensitive. At a constant bias of 0.8 V and on illumination

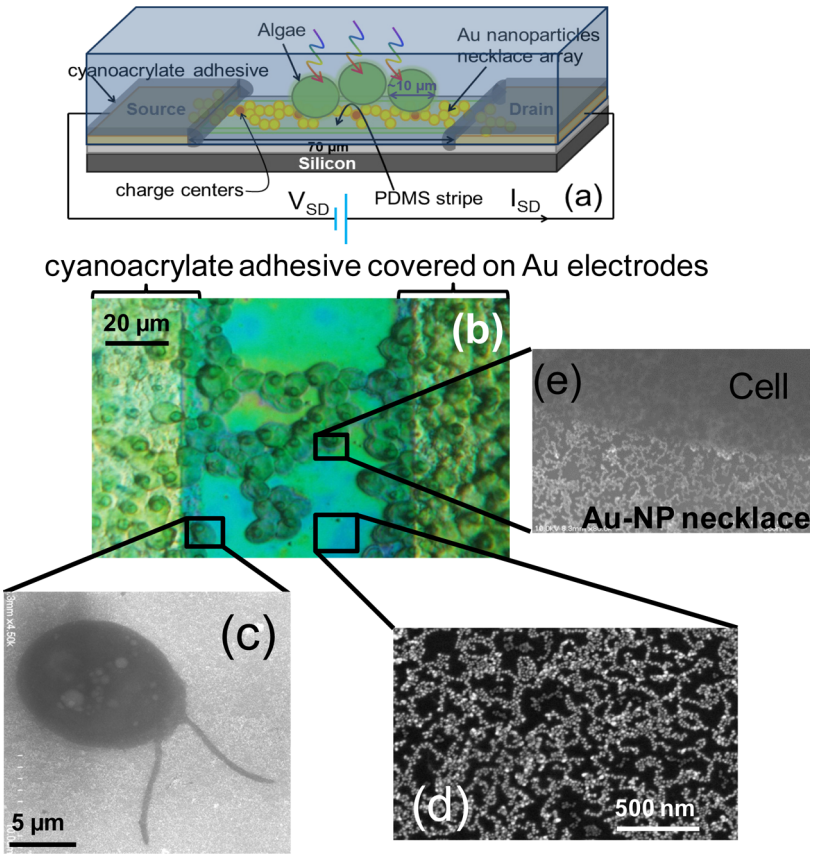


**Figure 1. Single-electron e-FET device in solution: (a) schematic of algae on the nanoparticle necklace network e-FET device; (b) optical microscope image of the device where algae were deposited between the hermetically sealed Au electrodes; (c) scanning electron microscope (SEM) image of an isolated alga on the necklace array; (d) SEM image of nanoparticle necklace network; (e) SEM image of necklace network in contact with algae.**

from a Hg-lamp in the 350 to 800 nm range, the device current, $I_{SD}$, between the source and the drain modulates when turning the light ON/OFF (Figure 2b). When the light is turned ON, the current increases by $\Delta I_{SD} \approx 20$ pA (Figure 2b, inset) to reach a constant value and reversibly decays to the original current levels when the light is turned OFF. The rise and decay in current takes about a minute. The characteristic time of the device current is consistent with the modulation in the thylakoid membrane potential caused by a light-driven proton gradient across the membrane during photosynthesis.[36]

The light induced excursion of the membrane potential is a reaction which occurs in all plant cells including algae but the explanation is still controversial, especially the complex ion fluxes through the membranes that may not be synchronous.[37] To first order, the mechanism of the current change due to modulation in the cell membrane potential is explained by considering the primary process of the light-induced photosynthetic proton flux in the thylakoid membrane. In the presence of light, the protons are transported into the thylakoid lumen as a result of photosynthesis and slowly return to the stroma after the light is OFF.[38] A schematic of the photosynthetic process pertinent to the biogating process is described in the SI (Figure C). The light-stimulated charging process relative to a no-light situation is schematically shown in Figure 2c. Transport of the light-induced photosynthetic proton gradient into the thylakoid lumen increases the pH of the stroma (in the chloroplast) to induce (more) positive charge in the EDL around the chloroplast (Figure 2c). The charging of the chloroplast by positive ions (*e.g.*, $K^+$ or $Mg^{2+}$) decreases the potential of the cytosol to increase the current as expected from Figure 2a. A simple model is developed to relate the modulation of pH in the stroma, $\Delta$pH to the cell membrane potential, and $\Delta\varphi$ due to the light-induced proton flux (eqs (1) through (10) in SI). For potential in mV, the model suggests $\Delta\varphi \approx 9\Delta$pH (eqs (9) and (10) in SI).

Typically, at a pH of ~7, the zeta potential of the cell is −25 mV. Thus, the $g_m$ is ~2.3 nS for the cell/device interface. For light-induced modulation of $\Delta I_{SD} \approx 20$ pA, the corresponding membrane potential modulation, $\Delta\varphi = \Delta I_{SD}/g_m$, is about −8.7 mV. (The negative sign signifies that the potential in the cytosol decreases (*e.g.*, hyperpolarizes) due to light.) We note in passing that no hydrolysis of water occurs during the continuous exposure to $V_{SD} = 0.8$ V for about 12 min (*i.e.*, the

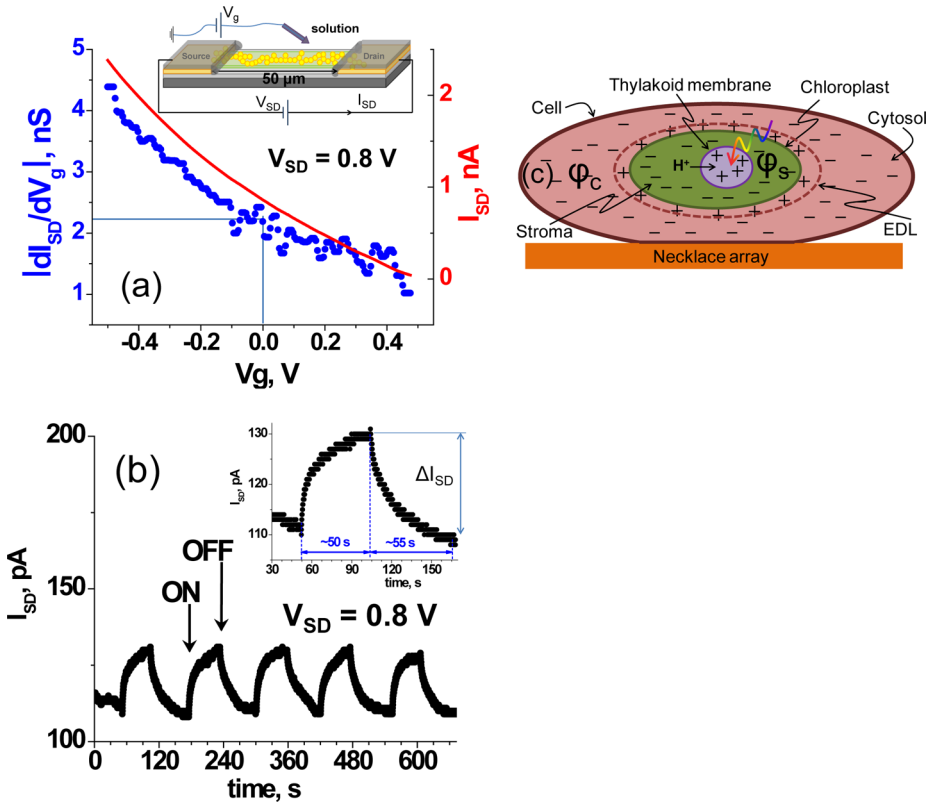


**Figure 2. Electronic behavior of eFET and eFET/algae device. (a) Transconductance behavior of the necklace array without algae. $V_g$ is applied *via* the Ag/AgCl reference electrode. (b) Modulation of the gating current due to light. The $\Delta I_{SD}$ is defined as the device current in an ON and OFF state. (c) The light induces photosynthetic proton transport into the lumen of the thylakoid making the chloroplast more negative, which is equivalent to applying $V_g < 0$. For both panels a and b, $V_{SD} = 0.8$ V. The charges in the schematic signify the change in the ion sign due to light exposure.**

duration of the experiment). Importantly, the biogating is exclusively due to the membrane potential because the ionic environment of the cell does not change. (A complication in quantifying electrophysiology studies where there is significant ion flux makes the method model dependent).[39] Thus, from the model (eq (10) in SI), $\Delta$pH $\approx$ 0.97, which is consistent with the literature.[38]

Next, we consider light stimulation in more detail. First, the effect of the light spectrum is studied. The device at fixed $V_{SD}$ = 0.8 V is exposed to monochromatic light from a four-grating spectrometer (see Methods), and $\Delta I_{SD}$ is recorded (Figure 3a). The current is normalized for the spectrum of the light source, that is, the $\Delta I_{SD}$ is divided by the intensity of light at the specific wavelength. The dynamic range of $\Delta I_{SD}$ over the 350 to 650 nm range (say at 600 nm relative to 375 nm) modulates over 2 orders of magnitude, indicating a very high specificity to photon energy (as expected). As $\Delta$pH $\approx \Delta I_{SD}$, the modulation in $\Delta$pH is also similar. The shape of the "biogating spectrum" nominally matches the absorption spectrum of the chlorophyll in terms of peak locations (Figure 3a). The chlorophyll is extracted from the cells with 99% of dimethylformamide. The discrepancy (in magnitude) between the biogating spectrum and the absorption spectrum is attributed to the complexity of the photochemical process, for example, the role of other pigments, such as carotenoids, that are also responsible for light harvesting and absorb at a slightly different wavelength than chlorophylls. Chlorophyll absorbs violet, blue, and red wavelengths, whereas the carotenoids absorb UV and blue wavelengths. We do not understand the significant mismatch in the two spectra in the 650 to 700 nm range.

Second, we consider the electron transport process in the thylakoid membrane where the photosystem is embedded. It is well-known that by imbedding 2,5-dibromo-3-methyl-6-isopropyl-*p*-benzoquinone (DBMIB) in the thylakoid membrane, the photoelectron flow from plastoquinone (PQ) to cytochrome *b6f* complex (Cyt *b6f* complex) (Figure C, SI) is inhibited. The decrease in current by about 2 orders of magnitude by DBMIB-treated algae (Figure 3a) further supports the consistency between the biogating spectrum and photosynthesis.

Third, we considered the effect of pH on the photosynthesis process. Photosynthesis depends on extracellular pH because it affects the electron flow as well as the physiological property of the algae. The electron transfer triggered by PQ oxidation is significantly influenced by the changes in pH (Figure C, SI).[40]

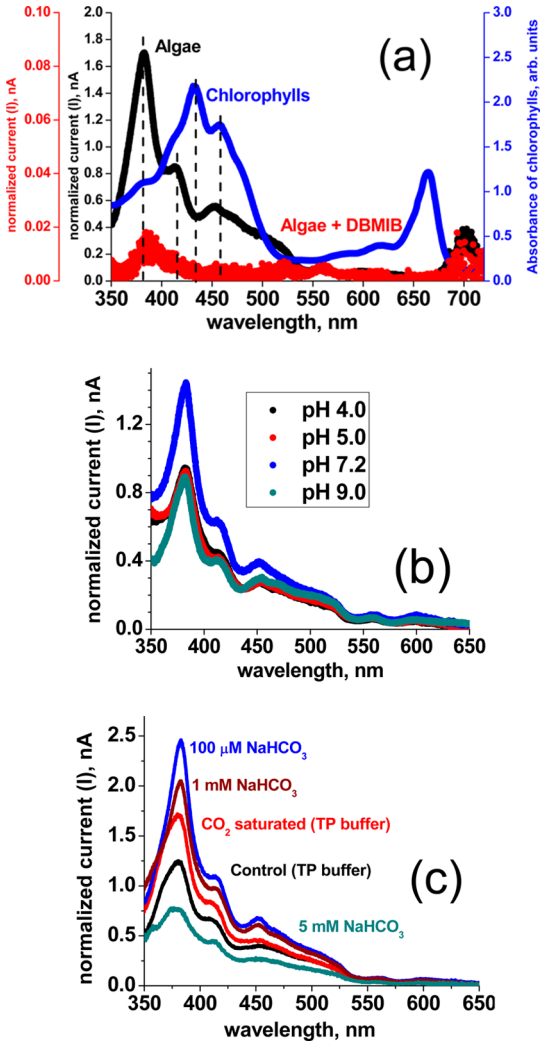


**Figure 3. Biogating spectrum for various stimuli. (a) Normalized device current, *I*, as a function of wavelength of excitation light (*i.e.*, biogating spectrum) (black line). Biogating spectrum of algae treated with DBMIB (red line). The absorption spectrum of chlorophylls extracted from algae (blue line). "Normalized" current implies that $I_{SD}$ is scaled for the intensity spectrum of the light source. (b) Biogating spectrum of algae in different pH solutions. TP buffers were adjusted with HCl or KOH solutions to pH 4.0−9.0. (c) Biogating spectrum as a function of the amount of carbon source in the media. TP buffers were adjusted with $CO_2$ gas or $NaHCO_3$ solution.**

The maximum oxidation occurs at pH 7.0 which is the optimum growth condition of algae in this study. The biogating spectrum for algae showing the optimum photosynthesis activity at a pH of 7.2 is, therefore, reasonable (Figure 3b).

Fourthly, we consider the effect of carbon concentration stimulation. The carbon source, particularly $CO_2$, is a limiting factor for the photosynthesis rate because of the low $CO_2$ affinity of RuBisCo (ribulose-1,5-bisphosphate carboxylase/oxygenase).[41] On an increase in the carbon concentration relative to the control by either saturating the solution with $CO_2$ or adding 0.1 mM $NaHCO_3$, the biogating current increases (Figure 3c). However, the $CO_2$-saturated buffer

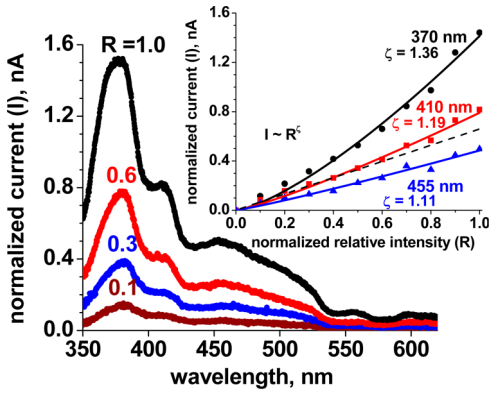


**Figure 4. Response of light intensity on photosynthetic activity. Biogating spectrum as a function of light intensity. The intensity ratio, $R = 1$, is defined at source on full power and $R = 0$ is off. The inset shows *I* as a function of *R* for three wavelengths. A power law fit to the data yields the scaling exponent, $\zeta$. The dashed line (black) is tangent to the response for 370 nm indicating the estimated linear behavior, that is, if $\zeta$ was 1.0.**

has an acidic pH of 5.6 that may adversely affect the photosynthesis activity, as observed in Figure 3b. As a result, the addition of $NaHCO_3$ than saturated $CO_2$ into the control solution with a pH of 7.2 is more effective. The highest photosynthetic biogating response observed is at 100 $\mu$M $NaHCO_3$, which is in agreement with studies on algae grown in ambient $CO_2$[42] and algal utilization of $HCO_3^-$ as a major form of inorganic carbon source.[43] Moreover, this result supports the $CO_2$ concentrating mechanism (CCM) model on the pH gradient across the thylakoid membrane in light. In light, the stoma has a pH of close to 8.0, whereas the thylakoid lumen has a pH of between 4 and 5 because of light-driven electron transport.[44] Under these conditions, $HCO_3^-$ is the predominant and favorable species in the stroma. A further increase in $NaHCO_3$ causes the photosynthesis activity to decrease due to the toxic effect of $Na^+$ on algae.

The complexity of photosynthesis is illustrated in the effect of light intensity on the biogating spectrum (Figure 4). The biogating spectrum, as a function of the fraction of maximum power to the source, R, scales monotonically. However, the relationship is not linear (Figure 4, inset). For the three prominent peaks, for example, at a wavelength of 370 nm, the normalized current, *I*, increases nonlinearly with respect to *R*. The scaling exponent, $\zeta \approx 1.36$ implies that photosynthetic activity (*i.e.*, *I*) at maximum power is 75% higher than the activity for $\zeta \approx 1$ (i.e., the linear dashed line). We do not understand the synergistic effect, but the nonlinearity is worth noting as it may be a critical factor in optimizing the algal culture for such as biofuel production.

## CONCLUSION

In summary, the single-electron eFET effectively and consistently responds to excursions of membrane

potential evoked by photosynthetic activity of algae in real time. The eFET is made from a 2D array of 1D nanoparticle necklaces comprising 10 nm Au particles. The rise in potential due to the photosynthetic process is about −8.7 mV. By modulating the wavelength in the 350 to 650 nm range, the photosynthetic activity is estimated to range over 2 orders of magnitude. The pH and carbon source are consistent with the photosynthetic process, indicating that the optimum activity occurs in a 100 $\mu$M $NaHCO_3$ solution and pH 7.2, respectively. By blocking the electron pathway in the thylakoid membrane, the photosynthetic activity, as expected, is reduced by about 2 orders of magnitude. As no secretion of ions occurs during the photosynthetic process, the biogating is exclusively due to membrane potential modulation. The necklace array device is fabricated by self-assembly and standard (conventional and soft) lithography methods that can be easily reproduced in other laboratories as a device to study biochemical processes in cells at high sensitivity in real time. Although we applied our system to determine photosynthetic algal properties, it can be very useful to probe physiological properties of other microorganisms and mammalian cells for applications such as in cancer drug discovery, interferon response, and analysis of genetic or biochemical functions of microorganisms with mutagenesis.

## METHODS

**Nanoparticle Necklace Network eFET Device Fabrication.** The nanoparticle necklaces are prepared by slowly mixing 1 mL of negatively charged 10 nm gold nanoparticles (BB international) with 50 $\mu$L of 20 mM $FeCl_3$ for 16 h. (Figure A). The device fabrication is described in the literature.[32] Briefly, a polydimethylsiloxane (PDMS, ~1 nm thick) strip is prepared using a contact printing method across two e-beam sputtered gold electrodes (230 $\mu$m (W) × 250 $\mu$m (L)), ~50 or 70 $\mu$m apart, on a silicon wafer. The width of the PDMS strip is ~30 $\mu$m. The PDMS strip was exposed to $NH_3$ plasma for 1 min to activate PDMS with positive charges. The gold nanoparticle necklaces are deposited onto the device for 18 h, resulting in a monolayer of a 1D necklace network (Figure B in SI and Figure 1d). The gold electrodes are hermetically sealed with a cyanoacrylate adhesive to prevent ionic current through the electrodes (Figure 1a).

**Algae Culture.** Light-induced biogating was demonstrated by coupling the array to the photosynthetic reaction of *Chlamydomonas reinhardtii* cc124. The strain cc124 was grown on TAP medium with pH 7.2 under continuous illumination of ~200 mmol photons $m^{-2}$ $s^{-1}$ (85 W SHO bulb, American Aquarium products) with an agitation of 100 rpm at 25 °C.

**Biogating Tests.** The cells (1−2 × $10^7$ cells/mL) were deposited on the poly (L-lysine)-coated Au nanoparticle necklace network eFET device (Figure 1). The device was placed into an electrochemical cell, and two working electrodes (WE1 and WE2) were connected to a bipotentiostat (PGSTAT 128N, Metrohm Autolab B.V.).[32] A Pt counter electrode and a 3 M Ag/AgCl reference electrode were inserted into the electrochemical cell. The device was operated in a TP buffer (pH 7.2, TAP without acetate) at a constant bias of 0.8 V. The light-induced modulation in current was measured under illumination of white light from a 200 W Hg arc lamp connected to a four-grating spectrometer (ACTON Spectrapro 2500i, Acton research corporation).

To demonstrate that light-induced biogating is involved in the electron flow of the photosynthetic reaction in the chloroplast's thylakoid membranes, the cells were exposed with 40 $\mu$M of 2,5-dibromo-3-methyl-6-isopropyl-*p*-benzoquinone (DBMIM) for 1 h, which inhibits electron transfer in photosynthetic reactions (Figure 3b). The action spectra of biogating responses to DBMIB were measured as previously described.

**Photosynthetic Biogating Responses to Light Intensity, Extracellular pH Change, And Inorganic Carbon Concentration.** To demonstrate the biogating responses to light intensity, extracellular pH changes and inorganic carbon concentration, the response-current were measured in TP buffers with different light intensity, pH values, or inorganic carbon concentration, as previously described. TP buffers were adjusted with HCl and KOH solutions for the desired pH levels or with $CO_2$ gas and $NaHCO_3$ for the desired dissolved inorganic carbon concentrations, respectively.

*Conflict of Interest:* The authors declare no competing financial interest.

*Acknowledgment.* We thank Dr. Chichao Yu for developing the device fabrication process to perform experiments in aqueous media. We thank Mr. Rahul Tevatia and Dr. Paul Blum for providing *Chlamydomonas reinhardtii* cc124. RFS would like to thank the Office of Basic Energy Science, DOE (DE-SC0001302), and NSF (CMMI-0926381) for financial support. About 60% of the funding is from the DOE.

*Supporting Information Available:* Additional figures, tables, results, and method description as described in the text. The Supporting Information contains three figures on the optical property of the necklaces, images of the device before algae deposition, the essential electronic process during photosynthesis, reproduction of Figure 2c, and a simple photosynthesis model to explain the light-induced biogating behavior. This material is available free of charge *via* the Internet at http://pubs.acs.org.

## REFERENCES AND NOTES

1. Froemke, R. C.; Poo, M. M.; Dan, Y. Spike-Timing-Dependent Synaptic Plasticity Depends on Dendritic Location. *Nature* **2005**, *434*, 221–225.
2. Sakmann, B.; Neher, E. Patch Clamp Techniques for Studying Ionic Channels in Excitable-Membranes. *Annu. Rev. Physiol.* **1984**, *46*, 455–472.
3. Stuart, G. J.; Hausser, M. Dendritic Coincidence Detection of EPSDs and Action Potentials. *Nat. Neurosci.* **2001**, *4*, 63–71.
4. Schulte, A.; Schuhmann, W. Single-Cell Microelectrochemistry. *Angew. Chem., Int. Ed.* **2007**, *46*, 8760–8777.
5. Chanda, B.; Blunck, R.; Faria, L. C.; Schweizer, F. E.; Mody, I.; Bezanilla, F. A Hybrid Approach to Measuring Electrical Activity in Genetically Specified Neurons. *Nat. Neurosci.* **2005**, *8*, 1619–1626.
6. Kralj, J. M.; Hochbaum, D. R.; Douglass, A. D.; Cohen, A. E. Electrical Spiking in *Escherichia coli* Probed with a Fluorescent Voltage-Indicating Protein. *Science* **2011**, *333*, 345–348.
7. Fromherz, P.; Offenhausser, A.; Vetter, T.; Weis, J. A Neuron-Silicon Junction: A Retzius Cell of the Leech on an Insulated-Gate Field-Effect Transistor. *Science* **1991**, *252*, 1290–1293.
8. Wrobel, G.; Seifert, R.; Ingebrandt, S.; Enderlein, J.; Ecken, H.; Baumann, A.; Kaupp, U. B.; Offenhausser, A. Cell-Transistor Coupling: Investigation of Potassium Currents Recorded with *p*- and *n*-Channel FETs. *Biophys. J.* **2005**, *89*, 3628–3638.
9. Zeck, G.; Fromherz, P. Noninvasive Neuroelectronic Interfacing with Synaptically Connected Snail Neurons Immobilized on a Semiconductor Chip. *Proc. Natl. Acad. Sci. U.S.A.* **2001**, *98*, 10457–10462.
10. Fromherz, P. Electrical Interfacing of Nerve Cells and Semiconductor Chips. *Chemphyschem* **2002**, *3*, 276–284.

11. Ingebrandt, S.; Yeung, C. K.; Krause, M.; Offenhausser, A. Cardiomyocyte-Transistor-Hybrids for Sensor Application. *Biosens. Bioelectron.* **2001**, *16*, 565–570.
12. Hai, A.; Shappir, J.; Spira, M. E. In-Cell Recordings by Extracellular Microelectrodes. *Nat. Methods* **2010**, *7*, 200–U50.
13. Pabst, M.; Wrobel, G.; Ingebrandt, S.; Sommerhage, F.; Offenhausser, A. Solution of the Poisson-Nernst-Planck Equations in the Cell−Substrate Interface. *Eur. Phys. J. E* **2007**, *24*, 1–8.
14. Rutten, W. L. C. Selective Electrical Interfaces with the Nervous System. *Annu. Rev. Biomed. Eng.* **2002**, *4*, 407–452.
15. Bruggemann, D.; Wolfrum, B.; Maybeck, V.; Mourzina, Y.; Jansen, M.; Offenhausser, A. Nanostructured Gold Microelectrodes for Extracellular Recording from Electrogenic Cells. *Nanotechnology* **2011**, *22*, No. Art. No. 265104.
16. Kim, W.; Ng, J. K.; Kunitake, M. E.; Conklin, B. R.; Yang, P. D. Interfacing Silicon Nanowires with Mammalian Cells. *J. Am. Chem. Soc.* **2007**, *129*, 7228–7229.
17. Keefer, E. W.; Botterman, B. R.; Romero, M. I.; Rossi, A. F.; Gross, G. W. Carbon Nanotube Coating Improves Neuronal Recordings. *Nat. Nanotechnol.* **2008**, *3*, 434–439.
18. Kim, J. H.; Kang, G.; Nam, Y.; Choi, Y. K. Surface-Modified Microelectrode Array with Flake Nanostructure for Neural Recording and Stimulation. *Nanotechnology* **2010**, *21*, No. Art. No. 085303.
19. Zhou, H. B.; Li, G.; Sun, X. N.; Zhu, Z. H.; Jin, Q. H.; Zhao, J. L.; Ren, Q. S. Integration of Au Nanorods with Flexible Thin-Film Microelectrode Arrays for Improved Neural Interfaces. *J. Microelectromech. Syst.* **2009**, *18*, 88–96.
20. Cohen-Karni, T.; Qing, Q.; Li, Q.; Fang, Y.; Lieber, C. M. Graphene and Nanowire Transistors for Cellular Interfaces and Electrical Recording. *Nano Lett.* **2010**, *10*, 1098–1102.
21. Hess, L. H.; Jansen, M.; Maybeck, V.; Hauf, M. V.; Seifert, M.; Stutzmann, M.; Sharp, I. D.; Offenhausser, A.; Garrido, J. A. Graphene Transistor Arrays for Recording Action Potentials from Electrogenic Cells. *Adv. Mater.* **2011**, *23*, 5045–5049.
22. Patolsky, F.; Timko, B. P.; Yu, G. H.; Fang, Y.; Greytak, A. B.; Zheng, G. F.; Lieber, C. M. Detection, Stimulation, and Inhibition of Neuronal Signals with High-Density Nanowire Transistor Arrays. *Science* **2006**, *313*, 1100–1104.
23. Vanmaekelbergh, D.; Houtepen, A. J.; Kelly, J. J. Electrochemical Gating: A Method to Tune and Monitor the (opto)Electronic Properties of Functional Materials. *Electrochim. Acta* **2007**, *53*, 1140–1149.
24. Arnold, M.; Cavalcanti-Adam, E. A.; Glass, R.; Blummel, J.; Eck, W.; Kantlehner, M.; Kessler, H.; Spatz, J. P. Activation of Integrin Function by Nanopatterned Adhesive Interfaces. *Chemphyschem* **2004**, *5*, 383–388.
25. Park, J.; Bauer, S.; von der Mark, K.; Schmuki, P. Nanosize and vitality: $TiO_2$ Nanotube Diameter Directs Cell Fate. *Nano Lett.* **2007**, *7*, 1686–1691.
26. Lu, W.; Xie, P.; Lieber, C. M. Nanowire Transistor Performance Limits and Applications. *IEEE Trans. Electron Devices* **2008**, *55*, 2859–2876.
27. Parrish, K. N.; Akinwande, D. Impact of Contact Resistance on the Transconductance and Linearity of Graphene Transistors. *Appl. Phys. Lett.* **2011**, *98*, 183505.
28. Cohen-Karni, T.; Timko, B. P.; Weiss, L. E.; Lieber, C. M. Flexible Electrical Recording from Cells Using Nanowire Transistor Arrays. *Proc. Natl. Acad. Sci. U.S.A.* **2009**, *106*, 7309–7313.
29. Dankerl, M.; Hauf, M. V.; Lippert, A.; Hess, L. H.; Birner, S.; Sharp, I. D.; Mahmood, A.; Mallet, P.; Veuillen, J. Y.; Stutzmann, M.; *et al.* Graphene Solution-Gated Field-Effect Transistor Array for Sensing Applications. *Adv. Funct. Mater.* **2010**, *20*, 3117–3124.
30. Kane, J.; Inan, M.; Saraf, R. F. Self-Assembled Nanoparticle Necklaces Network Showing Single-Electron Switching at Room Temperature and Biogating Current by Living Microorganisms. *ACS Nano* **2010**, *4*, 317–323.
31. Maheshwari, V.; Kane, J.; Saraf, R. F. Self-Assembly of a Micrometers-Long One-Dimensional Network of Cemented Au Nanoparticles. *Adv. Mater.* **2008**, *20*, 284–287.
32. Yu, C. C.; Lee, S. W.; Ong, J.; Moore, D.; Saraf, R. F. Single Electron Transistor in Aqueous Media. *Adv. Mater.* **2013**, *25*, 3079–3084.
33. Middleton, A. A.; Wingreen, N. S. Collective Transport in Arrays of Small Metallic Dots. *Phys. Rev. Lett.* **1993**, *71*, 3198–3201.
34. Narumi, T.; Suzuki, M.; Hidaka, Y.; Kai, S. Size Dependence of Current-Voltage Properties in Coulomb Blockade Networks. *J. Phys. Soc. Jpn.* **2011**, *80*, 114704.
35. Kane, J.; Ong, J.; Saraf, R. F. Chemistry, Physics, and Engineering of Electrically Percolating Arrays of Nanoparticles: A Mini Review. *J. Mater. Chem.* **2011**, *21*, 16846–16858.
36. Junge, W. Membrane-Potentials in Photosynthesis. *Annu. Rev. Plant Physiol. Plant Mol. Biol.* **1977**, *28*, 503–536.
37. Shabala, S.; Newman, I. Light-Induced Changes in Hydrogen, Calcium, Potassium, and Chloride Ion Fluxes and Concentrations from the Mesophyll and Epidermal Tissues of Bean Leaves. Understanding the Ionic Basis of Light-Induced Bioelectrogenesis. *Plant Physiol.* **1999**, *119*, 1115–1124.
38. Pennisi, C. P.; Greenbaum, E.; Yoshida, K. Analysis of Light-Induced Transmembrane Ion Gradients and Membrane Potential in Photosystem I Proteoliposomes. *Biophys. Chem.* **2010**, *146*, 13–24.
39. Peitz, I.; Fromherz, P. Electrical Interfacing of Neurotransmitter Receptor and Field Effect Transistor. *Eur. Phys. J. E* **2009**, *30*, 223–231.
40. Finazzi, G. Redox-Coupled Proton Pumping Activity in Cytochrome *b(6)f*, as Evidenced by the pH Dependence of Electron Transfer in Whole Cells of *Chlamydomonas reinhardtii*. *Biochemistry* **2002**, *41*, 7475–7482.
41. Spreitzer, R. J.; Salvucci, M. E. Rubisco: Structure, Regulatory Interactions, and Possibilities for a Better Enzyme. *Annu. Rev. Plant Biol.* **2002**, *53*, 449–475.
42. Badger, M. R.; Kaplan, A.; Berry, J. A. Internal Inorganic Carbon Pool of *Chlamydomonas reinhardtii* - Evidence for A Carbon-Dioxide Concentrating Mechanism. *Plant Physiol.* **1980**, *66*, 407–413.
43. Imamura, M.; Tsuzuki, M.; Shiraiwa, Y.; Miyachi, S. Form of Inorganic Carbon Utilized for Photosynthesis in *Chlamydomonas reinhardtii*. *Plant Cell Physiol.* **1983**, *24*, 533–540.
44. Moroney, J. V.; Ynalvez, R. A. Proposed Carbon Dioxide Concentrating Mechanism in *Chlamydomonas reinhardtii*. *Eukaryotic Cell* **2007**, *6*, 1251–1259.